

Irreversibility Field and Flux Pinning in MgB₂ with and Without SiC Additions

M.D. Sumption¹, M. Bhatia¹, E.W. Collings¹, M. Rhindfliesh²,
M. Tomsic², Y. Hascicek³, and S.X. Dou⁴

¹ LASM, Materials Science and Engineering Department,
OSU, Columbus, OH 43210, USA

²Hyper Tech Research, Inc. Columbus, OH 43210, USA

³The National High Magnetic Field Laboratory, Tallahassee FL, USA
ISEM, The University of Wollongong, Australia

Abstract

Critical current density was measured at 4.2 K for MgB₂ strands with and without SiC additions. In some cases measurements were performed on longer (1 m) samples wound on barrels, and these were compared to magnetic measurements. Most measurements were performed on short samples at higher fields (up to 18 T). It was found that in-situ processed strands with 10% SiC additions HT at 700-800°C show improved H_r and F_p values as compared to control samples, with H_r increasing by 1.5 T. At 900°C even larger improvements are seen, with H_r reaching 18 T and F_p values maximizing at 20 GN/m³.

Keywords: MgB₂, SiC, H_r , Flux Pinning

Introduction

Many groups now fabricate MgB₂ wires [1-13], and PIT strands are very promising for current carrying applications. Typical present day strands incorporate Fe or Cu, with perhaps Cu-Ni or monel as an outer sheath. There are two main variants for PIT MgB₂ fabrication, ex-situ [1-4], and in-situ [6,10-13]. Each of these choices has some advantages and some disadvantages, we focus here on in-situ powders, aiming to look at the influence of SiC on H_r and flux pinning, and to differentiate its influences in these two areas. Below we give a short background on MgB₂ strands, with an emphasis on H_r to put the present efforts in context.

Background

Grasso [1] using an *ex-situ* powder method to make MgB₂ tapes, found an irreversibility field, H_r , (the field at which the bulk current density goes to zero) just slightly higher than 12 T for field perpendicular to the tape face. An anisotropy factor of about 1.4 in H_r has been reported for tapes (with the parallel orientation being higher than the perpendicular one [2]), indicating that rolling partially aligns the Mg and B planes parallel to the broad face of the tapes. Suo and Flukiger, using the ex-situ technique H_{c2s} of 11.9 and 15.1 T at 4 K for H_{\perp} and H_{\parallel} (with a tape anisotropy of 1.3) [3]. Irreversibility fields were 8 and 10.4 T were measured at 4 K for H_{\perp} and H_{\parallel} , respectively [4]. Ball milling of MgB₂, also extensively employed by Flukiger [4] was seen to increase H_r and J_c .

Matsumoto and Kumakura [6] investigated the use of SiO₂ and SiC in the *in-situ process*, finding that they were effective in improving J_c considerably, as well as enhancing H_r substantially. In this particular case, J_c was sometimes increased by an order of magnitude with additions to make J_c values of 1600-6500 A/cm² at 12 T, 4 K, with H_r increasing from about 17 T to about 23 T at 4 K. Matsumoto and Kumakura [7] also tried ZrSi₂, ZrB₂ and WSi₂ additions to good effect. In a series of important papers Dou et al showed that SiC can significantly improve the properties of wires [14-16], although whether this is by improvements in pinning, or enhancements in the upper critical field, H_{c2} , as has been seen for thin films [18,19] is still not certain. This is the focus of the present work.

The Upper Critical Field, H_{c2} , and its Enhancement through Impurity Scattering

Upper Critical Fields in Conventional Single-Band Superconductors

For dirty non-paramagnetically limited single-band low temperature superconductors a well known formula for $H_{c2}(0)$ at zero temperature can be obtained by starting with Maki's dirty-limit H_{c20} and inserting an expression for the BCS zero-K thermodynamic critical field, H_{c0} , and find [20]

$$H_{c20} = 3.06 \times 10^4 \gamma \rho T_c \quad (1)$$

where ρ is the impurity resistivity and γ the electronic specific heat coefficient. Alternatively we can predict a value for H_{c20} from the slope of H_{c2} at T_c . This time we begin with a Maki dirty-limit nonparamagnetic theory but at $T = T_c$. We combine the Maki $(dH_{c2}/dT)_{T_c}$ with the BCS $(dH_{c0}/dT)_{T_c}$ [20] and find first of all that

$$\left(\frac{dH_{c2}}{dT} \right)_{T_c} = 4.49 \times 10^4 \rho \gamma \quad (2)$$

Finally by combining (2) with (1) we obtain the frequently quoted expression:

$$H_{c20} = 0.68 T_c \left(\frac{dH_{c2}}{dT} \right)_{T_c} \quad (3)$$

Equations (1) and (2) taken together in the form

$$\rho = \frac{3.27 \times 10^{-5}}{\gamma} \left(\frac{H_{c20}}{T_c} \right) = \frac{2.23 \times 10^{-5}}{\gamma} \left(\frac{-dH_{c2}}{dT} \right)_{T_c} \quad (4)$$

show that for single band superconductors both the slope H_{c20}/T_c and $(-dH_{c2}/dT)_{T_c}$ scale with ρ , and hence that (for fixed T_c) both the low temperature H_{c2} and that near T_c benefit simultaneously from an increase in ρ . Some treatments of the subject prefer to treat ρ in terms of an electron diffusivity, $D (= v_F^2 \tau / 3)$, where τ is the impurity-scattering relaxation

time) such that $1/\rho = e^2 N_F D$, in which case the scaled benefits to H_{c20}/T_c and $(-H_{c2}/dT)T_c$ are seen to vary as $1/D$.

Equation (3) suggests an experimental method of obtaining H_{c20} (which may be outside the range of many laboratory magnets) that can be carried out at moderate fields, near T_c . Equations (1)–(4) indicate that across-the-board increases in H_{c2} can be expected to follow increases in impurity resistivity, ρ , – a rule which has helped to guide the design of low temperature superconductors over the years. But whereas it is qualitatively true also for MgB₂ the simple rule has quantitative variants, for example: (i) some MgB₂ samples with comparable H_{c2} s have been found to have very different ρ s – an Eqn. (1) departure. (ii) Some experimentally measured H_{c20} s have been found to be considerably greater than the $(dH_{c2}/dT)_{T_c}$ -predicted values – an Eqn (3) departure.

Upper Critical Fields of MgB₂ -- General Responses to Changes in D_σ and D_π

Although Eqn. (3) predicts an H_{c20} some 68% below a linear back extrapolation of the $H_{c2}(T)$ vs T line near T_c , measurements on some MgB₂ samples have yielded H_{c20} values that lie close to and even above that extrapolation. With reference to a copious body of experimental results, Gurevich et al [21], based on the detailed analysis of Gurevich [22], have been able to further illustrate and explain this behavior in terms of the electronic diffusivities D_π and D_σ associated with MgB₂'s two-band conductivity:

$$\sigma = e^2 (N_{F\pi} D_\pi + N_{F\sigma} D_\sigma) \quad (5)$$

As explained by the above authors, the introduction of two diffusivities results in pronounced departures from the single-band predictions. In particular (H_{c2}/T_c) and $(-dH_{c2}/dT)_{T_c}$ respond individually to D_π and D_σ rather than together and in proportion to $1/D$. Thus, according to Gurevich et al [21] and to a first approximation:

$$H_{c2\text{near}T_c} \propto \frac{1}{\lambda_1 D_\sigma + \lambda_2 D_\pi} \quad (6)$$

where the λ s are the coupling constants and

$$H_{c20} \propto \frac{1}{\sqrt{D_\sigma D_\pi}} \quad (7)$$

Simply stated, near T_c H_{c2} varies inversely as the weighted arithmetic mean of D_σ and D_π while H_{c20} varies inversely as their geometric mean. Thus while increasing impurity scattering is beneficial to H_{c2} over the entire temperature range for both single-band and two-band superconductors, in the latter case (and recognizing the independence of D_π and D_σ) it offers H_{c20} the opportunity to diverge to very large values -- well beyond the 68% of the $(-dH_{c2}/dT)_{T_c}$ extrapolation -- in response to strong decreases in either D_σ or D_π .

Detailed Responses to D_σ D_π Inequalities

Suppose, as has turned out to be the case for dirty MgB₂ films, that $D_\pi \ll D_\sigma$ (i.e. π scattering much stronger than σ scattering) then Eqn. (6) approximates to

$$H_{c2 \text{ near } T_c} \propto \frac{1}{\lambda_1 D_\sigma} \quad (8)$$

In general $H_{c2 \text{ near } T_c}$ is controlled by the greater of the two diffusivities in this case D_σ . Further changes in $H_{c2 \text{ near } T_c}$ would expect to follow a manipulation of D_σ . On the other hand, since in Eqn. (7) D_σ and D_π are still tied together as a product (even though D_π is the “dominant” component), manipulation of either of them would seem to influence H_{c20} . But examination of the H_{c20} relationship in more detail reveals that for very different diffusivities

$$H_{c20} \propto \frac{1}{D_\sigma} \quad D_\sigma \ll D_\pi \quad (9)$$

and

$$H_{c20} \propto \frac{1}{D_\pi} \quad D_\pi \ll D_\sigma \quad (10)$$

So H_{c20} is controlled by the **smaller** of the two diffusivities – the D_π in dirty MgB₂ films.

H_{c2} Anisotropy

We conclude with a note on the effects of scattering on changes in H_{c2} anisotropy. Equations (6) and (7) refer to the field-perpendicular (to the basal plane, a - b) orientation. For the field-parallel orientation (c -direction), the diffusivities must be transformed, for example by $D_\sigma = \sqrt{(D_\sigma^{ab} D_\sigma^c)}$ and the same for D_π . Let us consider the anisotropy parameter $\gamma = H_{c2\parallel}/H_{c2\perp}$ at low temperatures and high temperatures on the assumption that $D_\pi \ll D_\sigma$, as in the case of dirty MgB₂ film. A temperature dependent H_{c2} anisotropy arises via the differing anisotropies of D_σ and D_π coupled with the fact that in this case D_π controls H_{c20} while D_σ controls H_{c2} near T_c . It can be shown (and is to be expected intuitively) that the diffusivity in the 3-D π band is less anisotropic than that in the 2-D σ band and thus γ decreases as the temperature decreases. Thus the enhancement of H_{c20} and the softening of its anisotropy is a consequence of the two-band character of MgB₂ coupled with a $D_\pi \ll D_\sigma$.

Experimental

Sample preparation

A CTFE process was used to produce MgB₂/Fe composite strand [10,11]. The starting Mg powders were 325 mesh 99.9% pure, and the B powders were amorphous, 99.9% pure, and at a typical size of 1–2 μm . The powders were V-mixed and then run in

a planetary mill; in some cases nano-size SiC powders were added. After powder preparation, a tube mill was used to continuously dispense the powder onto a strip of high purity Fe. This, after closing, was inserted into a monel or Cu-30Ni tube. Heat treatments were then performed under Ar. Ramp up times were typically x h, and the samples were furnace cooled. The times and temperatures at the plateau ranged from 675-850°C, for times between 5-30 minutes.

Measurements

Four-point transport J_c measurements were made on two sample types, short samples and barrel samples. The short samples were 3 cm in length, with a gauge length of 5 mm). The barrels had a single layer of wire, with each turn separated from its neighbors. The ends were soldered onto Cu end-rings, and the current leads were attached over a 1 m segment of strand. The voltage taps were 50 cm apart. Standard Pb–Sn solder was used for forming the contacts, and the J_c criterion was 1 $\mu\text{V}/\text{cm}$. Most measurements were made at 4.2 K in background fields of up to 15 T (applied transverse to the strand). In a few cases, vibrating sample magnetization (VSM) measurements were made. The VSM system had a 9 T maximum field, and loop measurement times were typically 20 min in duration. Measurements were performed at 4.2 K.

Results

Transport and magnetic J_c s were measured at 4.2 K for a set of samples (Set I, see Table 1) with, and in one case without, SiC additions. The transport results were measured on barrel samples in this case (1 m segments of wire). These transport results were then converted to F_p , using $F_p = J_c B$, with the results displayed in Figure 1. Magnetic results were measured on short sections, and gave somewhat higher results. The most likely reason for this is the presence of inhomogenities along the length of the strand, resulting in an somewhat (artificially) suppressed F_p for the transport results. While this does display reasonable transport properties over 1 m lengths, the influence of SiC additions are unclear. This led to a new set of experiments, Set II. In order to limit the scatter generated by extrinsic defects, it was decided to measure short samples. However, transport measurements were chosen over magnetic, to insure that any SiC were present in the wires in a usable way.

Set II consisted of six strands, six with SiC, and six without (see Table 1). The HT schedules were similar, with temperatures of 700°C and 800°C, and times from 5 to 30 min. These strands were then measured for transport J_c at 4.2 K in fields of up to 15 T. The results are displayed in Figure 2 in the form of a Kramer plot. The superiority of the SiC samples is immediately clear. Linear extrapolations for all samples show a jump in the irreversibility field of between 1-2 T. Low current data was taken for samples SiC800/05 and NSC700/15 which show a high field (low current) deviation from linearity, however, these curves show the same jump in H_r . Clearly, SiC is increasing H_r , although any dependence of this effect on HT is unclear. Figure 3 shows this data in the form of an F_p curve. F_p , as well as H_r , is apparently increased by the SiC, at least near 4.2 K.

The last set of data was given a very short HT at an elevated temperature; about 5 minutes at 900°C. J_c for this sample is shown in Figure 4 for a variety of temperatures. However, we can immediately notice that H_r is at least 16 T – significantly higher than for Set II samples. This suggests that the higher temperature HT is (perhaps with the addition of SiC) enhancing H_r . Figure 5 shows a Kramer plot for this data, and we notice the high temperature tail of the plot, at 4.2 K, leads off to an H_r of about 18 T. F_p curves, now normalized to H_r , are presented in Figure 6. We see by comparison to Figure 3 that F_{pmax} seems to be enhanced. F_{pmax} for Figure 3 samples, even with SiC, are going to be less than 10 GN/m³, while that for Figure 6 data is 20 GN/m³. Not only that, but the field at which the maximum occurs is higher – in this case to more than 4 T – higher than that of Figure 3

Discussion and Conclusions

SiC clearly increases H_r at 4.2 K for the present samples. This is in agreement with the results of [16] where enhancements in high field J_c are seen, and furthermore c -axis and a -axis lattice parameters are modified by the inclusion of SiC. Additionally, an increase in F_p is seen. This is consistent with the TEM images of [16], which show an increased dislocation density. We also note that the saturation of the change in c -axis and a -axis parameters with SiC addition seen in [16] suggest a limit to the SiC influence. Looking to results of the same group on carbon nano-tube additions, this may be controlled by reaction temperature [17]. This would explain the significant improvements in H_r and F_p for higher reaction temperatures seen in Figures 4-6.

In summary, in-situ processed strands with 10% SiC additions HT at 700-800C show improved H_r and F_p values as compared to control samples, with H_r increasing by 1.5 T. At 900°C even larger improvements are seen, with H_r reaching 18 T and F_p values maximizing at 20 GN/m³. High field measurements are now needed, but it may be that SiC increases both B_{c2} and pinning.

Acknowledgements

This work was supported by a State of Ohio Technology Action Fund Grant.

References

- [1] G. Grasso, A. Malagoli, M. Modica, et al., Supercond. Sci. Technol. 16 (2003) 271–275.
- [2] G. Grasso, A. Malagoli, D. Marre, et al., Physica C 378–381 (2002) 899–902.
- [3] R Flükiger, P Lezza, C Beneduce, et al., Supercond. Sci. Technol. 16 (2003) 264–270
- [4] R Flükiger, H.L. Suo, N. Musolino, et al., Physica C (2003) 286–305.
- [5] D. Eyidi, O. Eibl, T. Wenzel, et al., Supercond. Sci. Technol. 16 (2003) 778–788.
- [6] A. Matsumoto, H. Kumakura, H. Kitaguchi, and H. Hatakeyama, Supercond. Sci. Technol. 16 (2003) 926–930.
- [7] Y. Ma, H. Kumakura, A. Matsumoto, et al., Supercond. Sci. Technol. 16 (2003) 852–856.
- [8] B A Glowacki, M Majoros, M Vickers, et al., Supercond. Sci. Technol. 16 (2003) 297–305

- [9] B.A. Glowacki, M. Majoros, M. Eisterer, et al., *Physica C* 387 (2003) 153–161.
- [10] E.W. Collings, E. Lee, M.D. Sumption, et al., *Rare Metal Mat. Eng.* 31 (6): 406-409 Dec. 2002.
- [11] E.W. Collings, E. Lee, M.D. Sumption, et al., *Physica C* 386 (2003) 555-559.
- [12] S. Soltanian, X.L. Wang, I. Kusevic, et al., *Physica C* 361, 84-90 (2001).
- [13] S. Soltanian, X.L. Wang, A.H. Li, et al., *Solid State Commun.* 124 (2002) 59-62.
- [14] S.X. Dou, A.V. Pan, S. Zhou, et al., *Supercond. Sci. Technol.* 15 (2002) 1587–1591.
- [15] A.V. Pan, S. Zhou, H. Liu and S. Dou, *Supercond. Sci. Technol.* 16 (2003) 639–644.
- [16] S.X. Dou, A.V. Pan, S. Zhou, et al., *Journal of Appl. Phys.* 94 (2003) 1850-1856.
- [17] S.X. Dou, W.K. Yeoh, J. Horvat, et al., *Appl. Phys. Lett.* 83 (2003) 4996-4998.
- [18] C.B. Eom, M.K. Lee, J. H. Choi, et al., J 2001 High Critical Current Density and Enhanced Irreversibility Field in Superconducting MgB₂ Thin Films *Nature* 411 558-60
- [19] C.B. Eom et al., *Nature* 411, 558 (2001)
- [20] E.W. Collings, *Applied Superconductivity, Metallurgy, and Physics of Titanium Alloys*, Vol. 1 (Plenum Press 1986)
- [21] A. Gurevich, Enhancement of the Upper critical Field by Nonmagnetic Impurities in Dirty Two-Gap Superconductors, *Phys. Rev.* “December 2002” 67, Issue: 18, 2003. pp. 184515-184515-13.
- [22] A. Gurevich, S. Patnaik, V. Braccini, et al., Very High Upper Critical Fields in MgB₂ Produced by Selective Tuning of Impurity Scattering, presented at EUCAS 2003, to be published 04) 59-62.

List of Tables

Table. 1. Strand Specifications.

List of Figures

Figure 1. Pinning force density (from transport and magnetic J_c) vs B at 4.2 K for Set I strands, including both short samples and barrel-wound strands with and without SiC.

Figure 2. Kramer plot for Set II strands, with and without SiC.

Figure 3. Pinning force density (from transport J_c) vs B at 4.2 K for set II strands, with and without SiC.

Figure 4. Transport J_c vs B at various temperatures for Set III strand, which had SiC.

Figure 5. Kramer plot for Set III strand (at several temperatures), which had SiC.

Figure 6. Pinning force density vs B at various temperatures for Set III strand, which had SiC.

Table 1. Strand Specifications

Name	Tracer ID	SiC?	HT	SC%	OD
Set I					
BNSC700/30		N	700/30	22.8	0.984
BSiC700/05		Y	700/5	24.6	0.836
MSiC700/5		Y	700/5	24.6	0.836
MSiC700/15		Y	700/15	24.6	0.836
Set II					
SiC700/30	256a	Y	700/30	27.5	0.827
SiC800/15	256a1	Y	800/15	27.5	0.827
SiC800/05	256a2	Y	800/05	27.5	0.827
NSC700/30	253b	N	700/30	24.1	0.791
NSC800/15	253b1	N	800/15	24.1	0.791
NSC700/15	253b2	N	700/15	24.1	0.791
Set III					
D	257	Y	700/5+900/5	XXX	XXX

Fig. 1

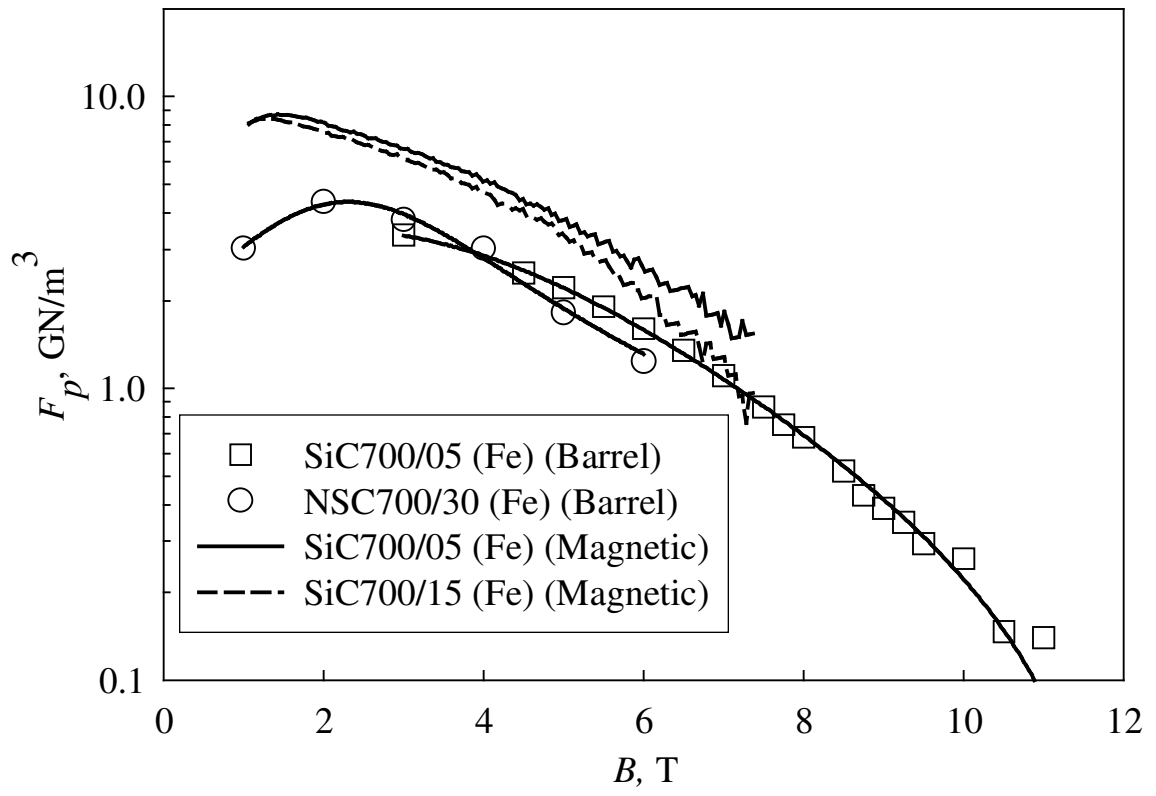


Fig. 2

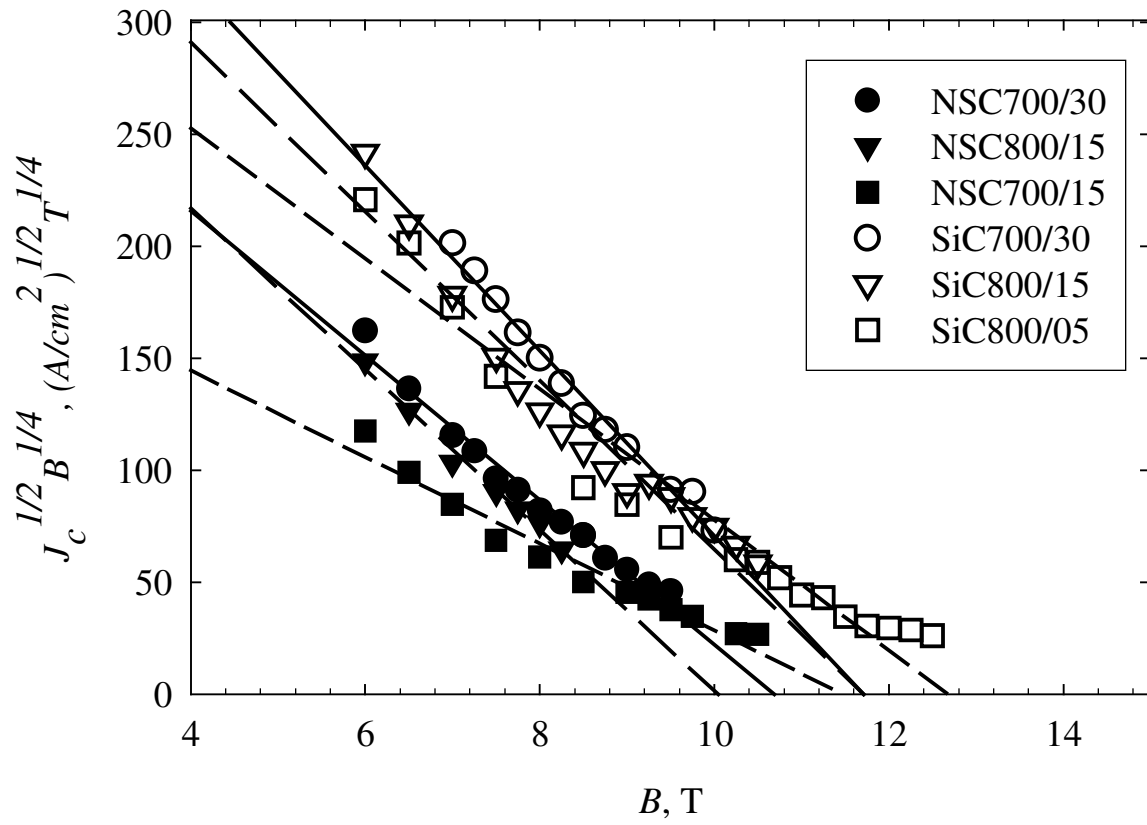


Fig. 3.

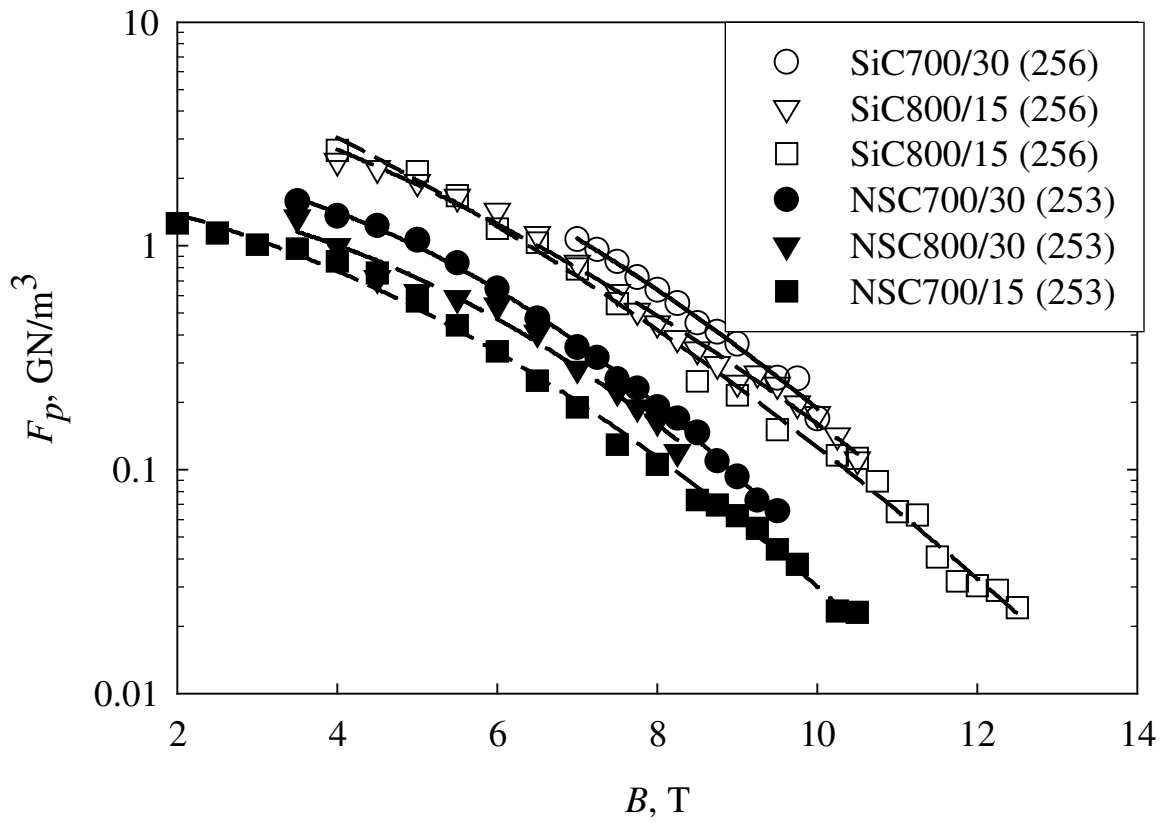


Fig. 4.

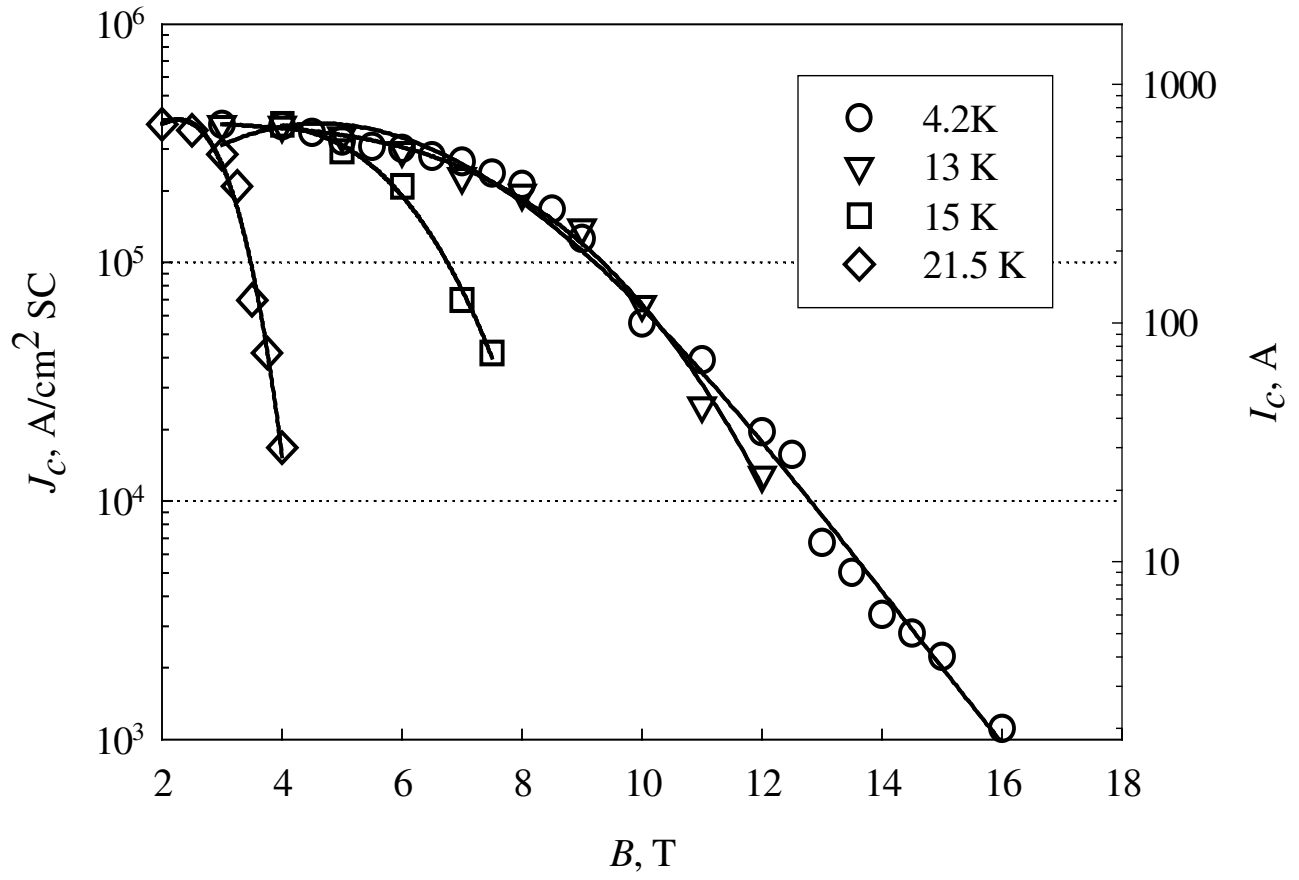


Fig. 5.

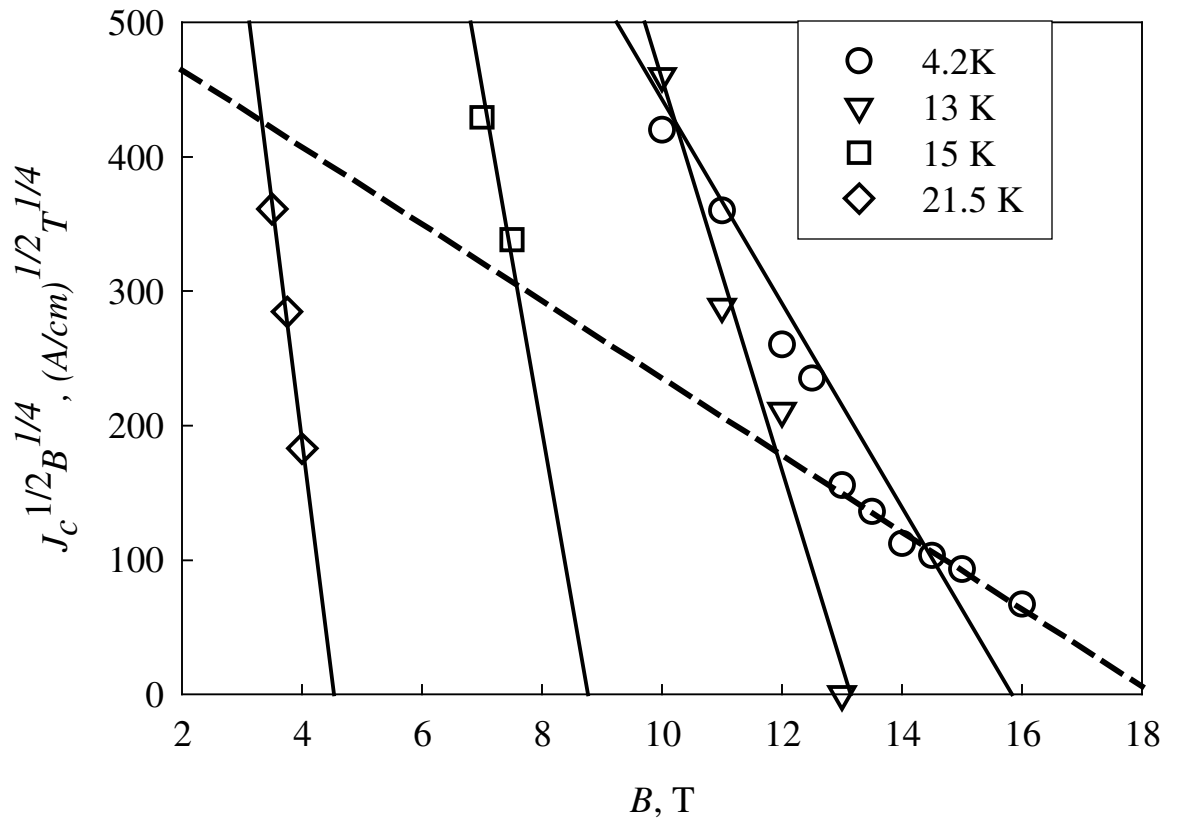


Fig. 6.

